remote sensing

MDPI

Article

Comparative Analysis between Sea Surface Salinity Derived from SMOS Satellite Retrievals and in Situ Measurements

Haodi Wang, Kaifeng Han, Senliang Bao, Wen Chen and Kaijun Ren *

Institute of Numerical Meteorology and Oceanography, College of Meteorology and Oceanography, National University of Defense Technology, Changsha 410073, China
* Correspondence: renkaijun@nudt.edu.cn

Abstract: Validating Sea Surface Salinity (SSS) data has become a key component of the Soil Moisture Ocean Salinity (SMOS) satellite mission. In this study, the gridded SMOS SSS products are compared with in situ SSS data from analyzed products, a ship-based thermosalinograph and a tropical moored buoy array. The comparison was conducted at different spatial and temporal scales. A regional comparison in the Baltic Sea shows that SMOS slightly underestimates the mean SSS values. The influence of river discharge overrides the temperature in the Baltic Sea, bringing larger biases near river mouths in warm seasons. The global comparison with two Optimal Interpolated (OI) gridded in situ products shows consistent large-scale structures. Excluding regions with large SSS biases, the mean ΔSSS between monthly gridded SMOS data and OI in situ data is –0.01 PSU in most open sea areas between 60°S and 60°N, with a mean Root Mean Square Deviation (RMSD) of 0.2 PSU and a mean correlation coefficient of 0.50. An interannual tendency of mean ΔSSS shifting from negative to positive between satellite SSS and in situ SSS has been identified in tropical to mid-latitude seas, especially across the tropical eastern Pacific Ocean. A comparison with collocated buoy salinity shows that on weekly and interannual scales, the SMOS Level 3 (L3) product well captures the SSS variations at the locations of tropical moored buoy arrays and shows similar performance with in situ gridded products. Excluding suspicious buoys, the synergetic analysis of SMOS, SMAP and gridded in situ products is capable of identifying the erroneous data, implying that satellite SSS has the potential to act as a real-time 27 Quality Control (QC) for buoy data.

Keywords: sea surface salinity; SMOS; moored buoy; in situ measurements

check for updates

Citation: Wang, H.; Han, K.; Bao, S.; Chen, W.; Ren, K. Comparative Analysis between Sea Surface Salinity Derived from SMOS Satellite Retrievals and in Situ Measurements. *Remote Sens.* **2022**, *14*, 5465. https://doi.org/10.3390/rs14215465

Academic Editor: Sergei Badulin

Received: 15 September 2022
Accepted: 26 October 2022
Published: 30 October 2022

Publisher's Note: MDPI stays neutral with regard to jurisdictional claims in published maps and institutional affiliations.

Copyright: © 2022 by the authors. Licensee MDPI, Basel, Switzerland. This article is an open access article distributed under the terms and conditions of the Creative Commons Attribution (CC BY) license (https://creativecommons.org/licenses/by/4.0/).

1. Introduction

Salinity is an Essential Climate Variable (ECV) in the Global Climate Observing System (GCOS) [1]. It critically influences the density of seawater, which drives the currents in the ocean, then influences the meridional transport of heat and materials and thus affects the ecosystems and earth climate. As a passive tracer, salinity has consistent spatial patterns with the horizontal evaporation-minus-precipitation (E-P) field in most areas of the sea surface. The structure and evolution of salinity depict how the freshwater inputs from precipitation, river runoff and glacier, etc., are redistributed throughout the ocean [2], and how these sea surface signals will run deep and affect the full volume of seawater by diffusive and advective processes [3]. Therefore, salinity has long been regarded as an indicator of the intensifying hydrological cycle under the global warming background [4,5]. In addition, as a key parameter in the equation of the state of seawater, salinity contributes to the changes of horizontal pressure gradients and vertical stability by altering density along with the temperature, which further influences the evolution of thermohaline circulation [6] and mixing processes [7]. These changes are closely related to air–sea fluxes and ultimately are associated with the change of earth climate [8]. For the above reasons, it is necessary to monitor, validate and analyze the variations of salinity to better understand their role in ocean dynamics and the hydrological cycle.

Spaceborne monitoring of Sea Surface Salinity (SSS) has the advantages of global coverage, high resolution and repeated measurement, providing unprecedented opportunities to track and resolve the mesoscale ocean structures from the sea surface directly, such as ocean fronts [9,10] and mesoscale eddies [11,12]. Over the past decade, the global SSS has been monitored by the Soil Moisture and Ocean Salinity (SMOS) satellite mission of the European Space Agency (ESA) since November 2009 [13,14], the Aquarius/SAC-D mission of the U.S. National Aeronautics and Space Administration (U.S. NASA) since June 2011 [15] and the Soil Moisture Active Passive (SMAP) satellite of NASA since January 2015 [16]. Comparatively, SMOS is advantageous in collecting a larger amount of brightness temperature data by utilizing different incidence angles at the same time [17], whereas SMAP and Aquarius are only capable of observing the ocean and ground targets at nearly fixed incidence angles [18]. However, SMOS suffers from more noise signals produced by Radio Frequency Interference (RFI), with the radiometric noise level significantly larger (from ~2.6K to 5K) [19] than SMAP (~1K) [20] and Aquarius (~0.12K) [21]. Recently, a number of approaches have been developed by the SMOS team to mitigate these contaminations [22–26], but the accuracy has not reached the 0.1 PSU target for a 10–30 day average and over an open sea of 200 km by 200 km. Moreover, the SSS retrievals are especially worrying in marginal seas, high latitudes and coastal areas [27–29], which require specific ΔSSS corrections based on using refined SSS validation results.

The density of near-surface in situ salinity measurements has witnessed a rapid increase after the launch of global Argo project in 1999 [30]. The currently available SMOS SSS data, both in the form of level 2 (L2) and level 3 (L3) products, have been validated against in situ measurements in a variety of circumstances. They may take the form of a direct comparison with co-located SSS measurements from Argo floats [31–33], thermosalinograph (TSG) [31,32,34–36] and saildrones [31], the comparison with data from tropical moored buoys array at seasonal scale [37,38] and the global and regional comparison with in situ analyzed products [27,34,39–45], as well as the SSS uncertainty estimations through a triple collocation of three independent SSS products [46,47]. However, the reliability of a comparison with both individual Argo floats and gridded Argo products has long been limited by the sparse sampling rate, especially near the coast [31,34,39,48], near large river mouths [41,42,49] and in the polar seas [32,35,36,40,43,50]. Another source of validation uncertainty is the larger footprints of satellite measurements compared with in situ measurements. SMOS provides the instantaneous measurements in a footprint of 40 km [51], whereas the in situ measurements represent the real-time observations at their precise point-based locations. The above issues are expected to be mitigated by using in situ SSS measurements with higher quality, wider distributions and higher density.

Previous validation efforts have generally ignored the long-term changes in the uncertainties of SSS despite the fact that more than 10 years of high-resolution SSS data have been accumulated by three satellite missions. Moreover, most previous studies tend to focus on single spatial and temporal scale. For example, the comparison with tropical moored buoys are mainly focused on the seasonal variations by extracting annual signals from harmonic analysis [37,38], which is also worth extending to the weekly and interannual scales. In addition, most in situ analyzed data products are monthly updated and have incorporated more in situ SSS measurements than the previous versions. However, the validation of SMOS L3 and L4 products against the newly released in situ analyzed SSS products has rarely been conducted in recent years. These products are expected to overcome the under-sampling of Argo-based products by incorporating a wider range of in situ measurements and reproducing the global SSS field at higher resolutions.

The objective of this study was to compare the SMOS L3 and L4 products with in situ SSS measurements at different time and space scales, against both individual SSS measurements and state-of-the-art in situ analyzed products. The unique advantage of each SSS data type was utilized to design the comparison strategy of this study, for example, the full spatial and temporal coverage of analyzed SSS products, the weekly time resolution of the tropical moored buoy data, and the abundance of SSS data collected by the World

Ocean Database (WOD) and ship-based SSS data in the Baltic Sea. The validation results presented by this study are expected to help identifying regions where SMOS SSS data should be used with caution and where the retrieval and correction algorithm should be improved.

This paper is organized as follows. Data and comparing methods are introduced in Section 2. The results of comparisons against in situ observational data in a typical marginal sea, in the global ocean and in the tropical areas are described in Section 3. The conclusions and discussions are presented in Section 4.

2. Data and Methods

2.1. SMOS Data

The version 2 SMOS SSS products developed by the Barcelona Expert Center (BEC) are used in this study [47]. The BEC SMOS SSS products are generated by using the de-biased non-Bayesian algorithm to eliminate systematic biases. Two global products were used in this study: the monthly binned products and 9-day running average L3 maps. The time range of SMOS BEC L3 v2.0 products was January 2011 to December 2019. Additionally, two Baltic+SSS products with the same time period were used: the daily generated 9d maps of L3 product in a 0.25 grid, and the daily L4 product with a spatial resolution of 0.05°. Based on the SSS anomalies generated from debiased non-Bayesian retrieval, the temporal variations of Baltic+SSS L3 data were calibrated by the CMEMS Baltic Sea physical reanalysis (PHY_003_011) product, and the spatial variations were corrected by using the regional SeaDataNet SSS climatology [47]. The Baltic+SSS L4 product was generated by a multifractal fusion over Baltic+SSS L3 SSS maps using ancillary Sea Surface Temperature (SST) data [52].

We also examined the consistency of SMOS SSS with other satellite retrievals. The JPL SMAP CAP V5.0 data were used due to its longer than 4-years' overlap and the same spatial resolution with SMOS data. This monthly mapped L3 product is based on the Combined Active-Passive (CAP) retrieval algorithm [53]. An enhanced calibration methodology was applied to calibrate L1 Brightness Temperature data to reduce the ascending–descending biases [54]. SMAP data begin in April 2015 and the monthly updating is ongoing.

2.2. In Situ Measurements

Two objectively interpolated (OI) in situ analyzed SSS products were utilized in this study. Both products overcome the inadequate spatial coverage of Argo-based products by incorporating extensive in situ SSS data collected by various sensors. The first are the ISAS-20 data provided by Ifremer, which are primarily based on Argo profiles and supplemented by in situ measurements from other databases (e.g., GADS and CCHDO) [55]. The inclusion of non-Argo data effectively reduces large-scale SSS uncertainties, especially in areas with a low Argo sampling rate such as strong stratification seas and near large estuaries [55,56]. The quality control of ISAS-20 data is achieved through objective analysis. The second product was a synthesized SSS dataset referred to as WODSSS, which is generated by appending the monthly SSS anomalies from the World Ocean Database 2018 (WOD18) to the corresponding monthly SSS climatology from the World Ocean Atlas 2018 (WOA18) [42,57]. The anomaly fields are generated by an average of quality-controlled salinity data provided by WOD18, which include Argo, CTDs, surface drifters, gliders and bottles data. Figure 1 shows that the in situ SSS data merged into two products have covered most of the global ocean. There are more than 100 SSS measurements within most $1^\circ \times 1^\circ$ grid cells between 60°N and 60°S, and more than 50 SSS measurements at most $0.25^\circ \times 0.25^\circ$ grids in the Baltic Sea. The supplement of non-Argo data compensates for the scarce Argo profiles in marginal seas. The shallowest layers of each product, which are 1m for ISAS-20 and 0m for WODSSS, were selected to compare with the skin salinity retrieved by SMOS [42,55,57]. To the best of our knowledge, there is no recent comparative analysis between SMOS products and the newly released ISAS-20 product, whereas the WODSSS product has been only used to validate the Aquarius SSS in [58].

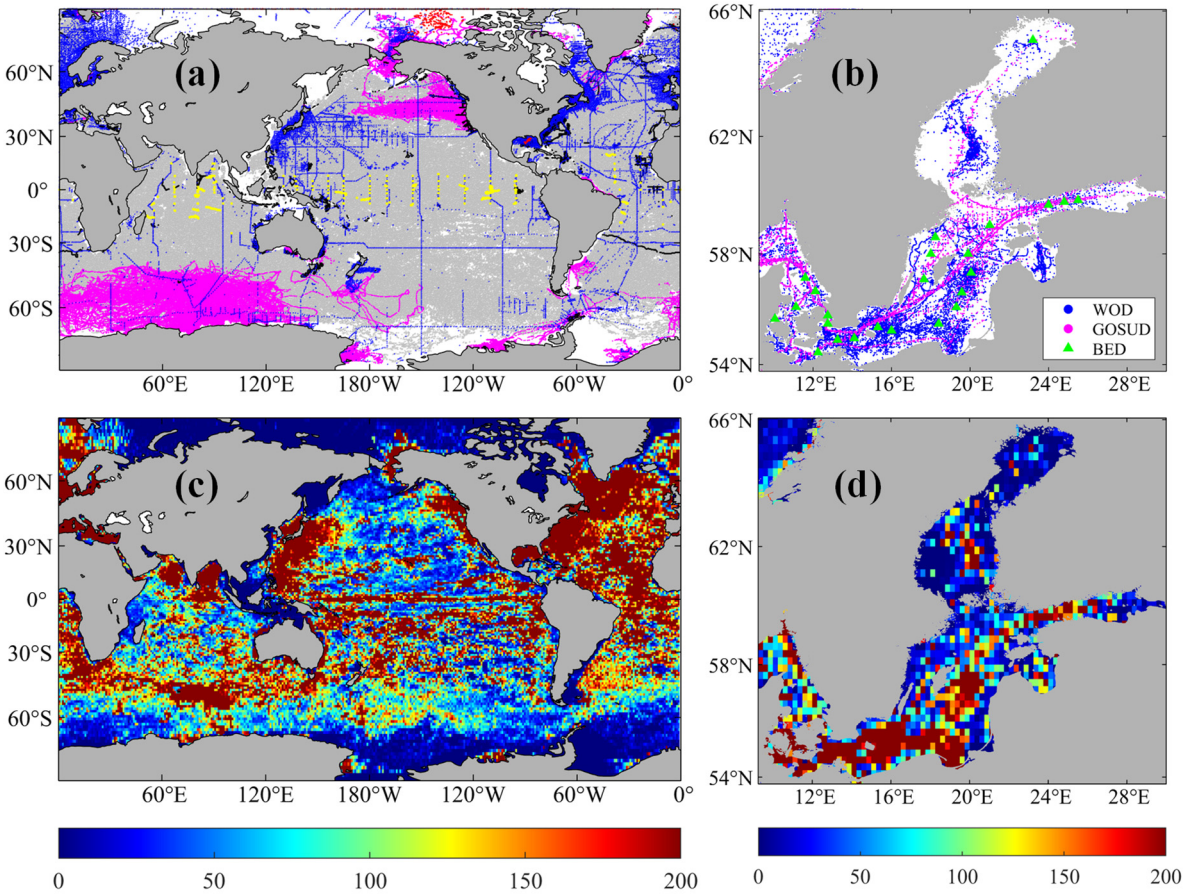


Figure 1. (**a**) Global distribution of in situ salinity data from the World Ocean Database (gray: Argo profilers, yellow: mooring buoys, blue: CTD, black: glider, red: drifting buoys, magenta: thermosalinograph). (**b**) Regional distribution of in situ salinity data in the Baltic Sea as provided by the GOSUD (magenta), the World Ocean Database (blue) and the Baltic Environmental Database (green). The bottom panels show the corresponding data volume of (**c**) the global WOD data at 1° boxes and (**d**) multi-source salinity measurements in the Baltic Sea at 0.25° boxes.

Due to the under-sampling of in situ equipment, the in situ analyzed SSS products may contain large uncertainties in the Baltic Sea [59]. Therefore, we explored individual SSS measurements from several publicly available ocean databases to support the comparative analysis in the Baltic Sea. One source was thermosalinograph (TSG) data from the Global Ocean Surface Underway Data (GOSUD) Project (http://gosud.org). The abundant TSG data were especially valuable in the Baltic Sea since Argo trajectories are rarely trapped in this semi-closed marginal sea. Another source of individual in situ SSS measurements was the World Ocean Database (WOD), which provides a large amount of uniformly formatted, quality-controlled SSS data collected by profilers, CTDs, gliders, bottles, ocean stations and drifting platforms. The third source was the Baltic Environmental Database (BED; http://nest.su.se/bed) developed by the Baltic Nest Institute, Stockholm, which contains long-term salinity records at fixed locations over the Baltic Sea.

2.3. Mooring Buoy

Long-term salinity records provided by the Global Tropical Moored Buoy Array (GTMBA) were used in this study. Each buoy provides continuous salinity measurements near sea surface (~1 m) in tropical regions with high temporal resolution during the whole SMOS period. The GTMBA consists of Tropical Atmosphere Ocean (TAO) data in the Pacific [60], the Pilot Research Moored Array in the Tropical Atlantic (PIRATA) [61] and the Research Moored Array for African-Asian Australian Monsoon Analysis and Prediction

(RAMA) in the Indian Ocean [62]. They record temperature and salinity every 10 minutes, and the raw data have been postprocessed into hourly data with an accuracy of 0.2 PSU [60]. To compare with satellite data, only surface salinity measurements (1 m) with the highest data quality (QC flag = 1) were used in this study. An 8-day moving average was applied to the postprocessed hourly data to ensure a consistent time resolution with the collocated SMOS data.

2.4. Data Collocation Method

As pycnoclines are generally deeper than 20 m in most areas of the Baltic Sea [63], here we considered the seawater above 5 m homogeneously mixed and representative of the sea surface. Based on this fact, we kept the shallowest measurement acquired between 0–5m depth to compare with SMOS data; in situ SSS data below 5 m were discarded to avoid large top–bottom salinity differences under heavy rainfall [64]. As for the spatial collocation, the location of each in situ data was gridded into the nearest grid cell of satellite, which is 0.25° for the L3 product and 0.05° for the L4 product. All in situ data corresponding to the same grid cell were averaged. As for temporal collocation, all the in situ data available in the 9 days used to generate the SMOS L3 product and in the same day of the L4 map were considered and averaged in the comparison. Finally, all the collocated data were interpolated into a uniform L3 grid and monthly resolution for comparison purposes. Only SSS data pairs meeting such constraint: $Q1 - 1.5 \times IQR < | OBS - SMOS | < Q3 + 1.5 \times IQR$ were selected to compute statistics [65]. Q1 and Q3 represented the first and third quartile of data series and the IQR was defined as $Q3 - Q1$. Data pairs out of this confidence range were regarded as outliers and discarded.

2.5. Strategy of Comparison

The comparative analysis of SSS in this study was primarily based on the calculation of fundamental statistic parameters, including the ΔSSS, the standard deviation, the Root Mean Square Deviation (RMSD), and the Pearson correlation coefficient together with p-value. The corresponding algorithm of each parameter is listed in Table 1.

Table 1. Specific algorithm for the fundamental statistic parameters used in this study.

Parameter	Algorithm
Mean	$\sum_{i=1}^{n} SSS_i$
ΔSSS	$SSS_{satellite} - SSS_{in\ situ}$ (1)
Standard Deviation	$\sqrt{\frac{\sum_{i=1}^{n}(SSS-\overline{SSS})^2}{n}}$ (2)
RMSD	$\sqrt{\frac{\sum_{i=1}^{n}(SSS_{satellite}-SSS_{in\ situ})^2}{n}}$ (3)
Correlation Coefficient [1]	$\frac{\sum_{i=1}^{n}(SSS_{satellite}-\overline{SSS}_{satellite})(SSS_{in\ situ}-\overline{SSS}_{in\ situ})}{\sqrt{\sum_{i=1}^{n}(SSS_{satellite}-\overline{SSS}_{satellite})^2 \cdot (SSS_{in\ situ}-\overline{SSS}_{in\ situ})^2}}$ (4)

[1] The *p*-value of the correlation coefficient was calculated by MATLAB toolbox with the significance level of 0.05.

The comparison strategy of this study is described as follows. First, the performance of SMOS retrievals under difficult SSS retrieval conditions was evaluated by a comparison in the Baltic Sea against the collocated in situ SSS measurements from three ocean databases. Retrieving SSS in the Baltic Sea was challenging due to a variety of technical difficulties, such as low sensitivity of radiometers in cold water, land–sea contaminations, freshwater influx and Radio-Frequency Interferences (RFI). Therefore, the regional assessment in the Baltic Sea helps us to figure out whether the SMOS satellite has good capacity to retrieve SSS under these extreme conditions, and whether the data quality of SMOS SSS products in subpolar marginal seas is high enough for scientific usage. Three different SMOS BEC products were validated: the global L3 product, the Baltic+SSS L3 product and

the Baltic+SSS L4 product. A preliminary assessment was first conducted to examine the error structure of each product by calculating the mean SSS values, standard deviation, ΔSSS and RMSD consistently on a 0.25° (L3) grid. Then, the best performing SSS product in the Baltic Sea was selected for further evaluation at seasonal scale, which was realized by estimating the ΔSSS and RMSD from all collocated SSS pairs in different seasons.

After that, we compared SMOS SSS with in situ SSS at different time and spatial scales. Taking ISAS-20 and WODSSS products as a reference, a global comparison was conducted by illustrating the spatial distribution of ΔSSS, RMSD and correlation coefficient from 60°N to 60°S excluding polar regions. We also analyzed the ΔSSS and RMSD structure at three different spatial resolutions, 0.25°, 1° and 5°, and make a comparison with SMAP data. Finally, in the tropical ocean, the SSS variations at weekly-to-interannual scales were compared against the long-term SSS records of GTMBA.

3. Results

3.1. Regional Comparison in the Baltic Sea

The density map (Figure 1d) shows that in situ SSS measurements covered most areas of the Baltic Sea. To eliminate the under-sampling areas, only grids with more than 10 collocated SSS pairs were selected for statistical calculations. The topography and subregions divided in the Baltic Sea are given in Figure 2.

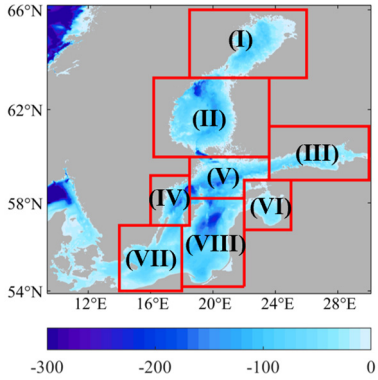


Figure 2. Eight subregions divided in the Baltic Sea, including (**I**) Bay of Bothnia, (**II**) Bothnia Sea, (**III**) Gulf of Finland, (**IV**) West Gotland Basin, (**V**) North Baltic Proper, (**VI**) Gulf of Riga, (**VII**) Bornholm Basin, (**VIII**) East Gotland Basin.

Figure 3 shows the spatial distribution of mean SSS and STD in the Baltic Sea obtained from three SMOS products and collocated in situ measurements. Their large-scale SSS patterns were generally consistent between satellite and in situ observations, including the fresh water in the Gulf of Bothnia, the high salinity water in Kategatte and Belt Sea, and the significant SSS front in the Baltic Proper. The SSS ranged from 3 to 8 PSU with a smooth negative gradient extending meridionally. The global L3 product showed the highest mean SSS value (6.19 PSU) and had the largest deviation from in situ measurements (5.58 PSU) compared with Baltic+SSS L3 (5.31 PSU) and L4 (5.47 PSU) data. In contrast, the STD patterns showed very significant differences. Higher mean STD value of 1.09 PSU was obtained from the SMOS global L3 product, which was more than twice as large as that of in situ measurements (0.54 PSU) and the Baltic+SSS products (0.56 PSU for L3 product and 0.34 PSU for L4 product). It suggests that the temporal noise of SMOS SSS in the Baltic Sea has been well smoothed by the temporal correction of Baltic+SSS products by using the CMEMS reanalysis product [47].

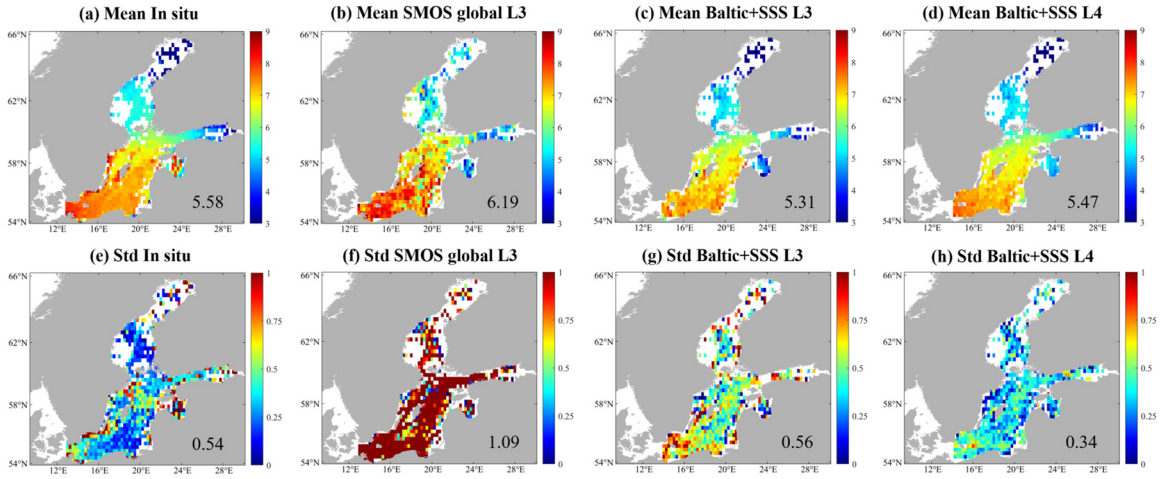


Figure 3. Mean SSS field in the Baltic Sea averaged from collocated (**a**) multi-source in situ salinity measurements. (**b**) BEC global L3 product, (**c**) Baltic+SSS L3 product and (**d**) Baltic+SSS L4 product on a consistent $0.25^\circ \times 0.25^\circ$ grid. The lower panels show the corresponding STD values of the collocated (**e**) multi-source in situ SSS measurements and (**f**) BEC global L3 product, (**g**) Baltic+SSS L3 product and (**h**) Baltic+SSS L4 product. The numbers labeled in the lowest right are the spatial average SSS values. The unit is in PSU.

Figure 4 shows the corresponding spatial distribution of ΔSSS and RMSD between three SMOS products and in situ measurements. The overall negative ΔSSS values were synchronously seen from both the Baltic+SSS L3 and L4 products, with the smaller ΔSSS and RMSDs belonging to the L4 product. Large ΔSSS and RMSD values were mainly distributed near the coast and in the gulfs, such as in the northern part of the Bay of Bothnia, in the Gulf of Riga and in the West Gotland Basin. In comparison, the global L3 products contained significantly larger positive biases, especially in the Bay of Bothnia, the East Gotland Basin, the North Baltic Proper and the Gulf of Riga, where several RMSD values reached as large as 2 PSU. Overall, the Baltic+SSS L4 product was closest to the in situ measurements in terms of mean fields and variances, as also supported by the smallest biases and RMSD values against collocated in situ SSS data.

To examine the performance of SSS retrievals at cold and warm seasons, Figure 5 presents the spatial ΔSSS and RMSD structures between collocated Baltic+SSS L4 SSS data and in situ SSS data at four boreal seasons. The corresponding density maps are attached in the left column, showing that the in situ SSS measurements were evenly distributed in the four seasons and their spatial distributions were generally consistent. The SSS measurements were abundant in the southern part of the Baltic Sea, but relatively scarce in some coastal areas, especially in the Bay of Bothnia, the Bothnia Sea and the West Gotland Basin. Statistics at these under-sampled locations should be treated with caution. For each season, the mean ΔSSS values were negative and the RMSDs were larger than 0.4 PSU, suggesting the Baltic+SSS L4 product underestimates the mean SSS over the basin throughout the year. Larger biases were mainly seen within the Gulf of Riga and the West Gotland Basin. Note that maximum biases and RMSDs appeared in summer, whereas minimum values appeared in winter. The Baltic Sea SSS retrieved from SMOS was significantly influenced by Sea Surface Temperature (SST) that influences the sensitivity of L-band sensor and river discharge that brings a large volume of freshwater [66]. Since the summer of Baltic Sea is characterized by higher SST reducing negative ΔSSS values and larger runoffs (Figure S5) producing negative ΔSSS values [67], the larger biases and RMSDs in summer indicate that the river runoff may play a dominant role in SSS retrievals of SMOS in the Baltic Sea rather than the SST.

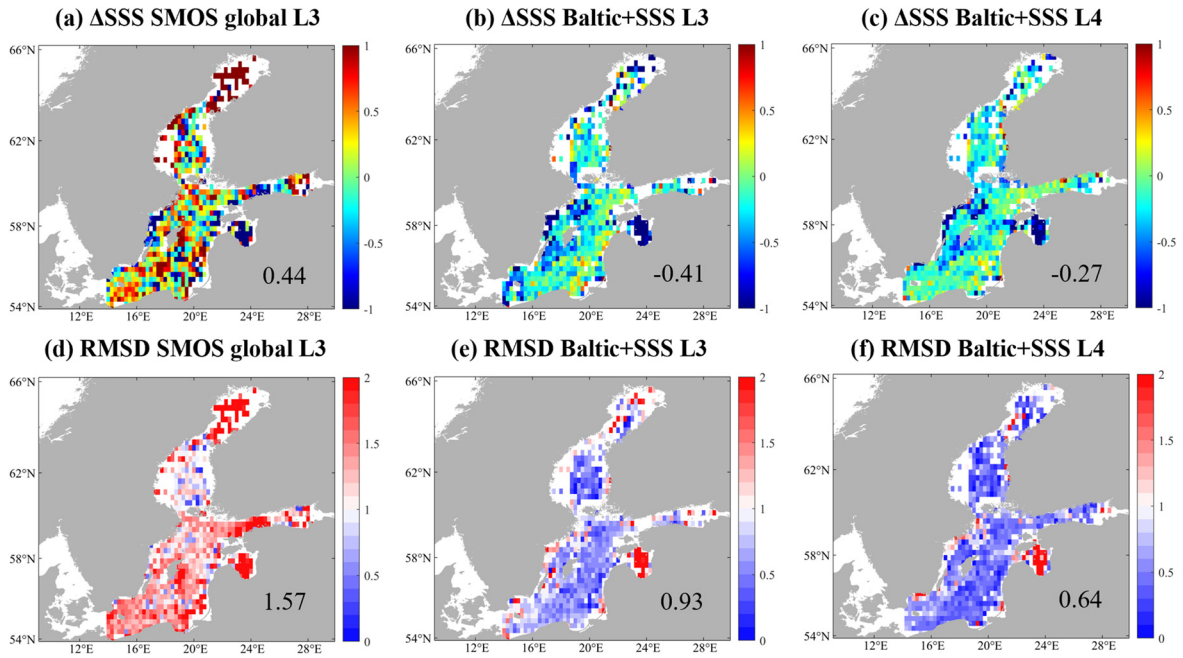


Figure 4. Horizontal distribution of mean ΔSSS (upper) and RMSD (bottom) values with respect to in situ SSS measurements. From left to right: BEC global L3 product, Baltic+SSS L3 product and Baltic+SSS L4 product. The numbers labeled in the lowest right are the spatial average RMSD values. The unit is in PSU.

Eight regions were divided in the Baltic Sea to evaluate the performance of SMOS SSS retrievals under different ocean conditions, including the Bay of Bothnia, the Bothnia Sea, the Gulf of Finland, the West Gotland Basin, the North Baltic Proper, the Gulf of Riga, the Bornholm Basin, and the East Gotland Basin (Figure 2). Statistics for each region are quantified respectively in Figure 6. The SSS was overall underestimated by SMOS in all the regions of the Baltic Sea. The majority of SSS pairs present theΔSSS values smaller than 1 PSU and the corresponding mean ΔSSS and RMSD value are no larger than –0.4 PSU and 0.8 PSU, respectively. Although affected by the freshwater of Neva, the largest river into the Baltic Sea, the smallest mean bias still belonged to the Gulf of Finland. The largest mean bias of –0.27 PSU was presented in the Gulf of Riga with a large RMSD of 0.65 PSU and the average number of in situ SSS data exceeding 100. Being surrounded by semi-closed topography, the large SSS differences here were possibly caused by a combined effect of land contaminations and the freshwater supplied by the Daugawa River from southeast. In addition, there are regions with large biases, large RMSDs and many missing values, such as the Bay of Bothnia, the Bothnia Sea and the West Gotland Basin, which resulted from the scarcity of in situ SSS measurements. Additional ship surveys are expected in these regions to achieve more refined comparison and validation.

Although statistics give optimistic results, they should be treated with caution. It is worth noting that in situ SSS observations located near the coast and inside the gulfs may carry large errors. For example, anomalous high and low values appeared at the adjacent grid points in the Gulf of Finland, and the same was true in the Gulf of Bothnia and the East Gotland Basin. Additionally, we emphasize that the above statistics were calculated from average SSS values on $0.25^\circ \times 0.25^\circ$ grid points, which only proves the effectiveness for the validation of the long-term mean SSS field in the Baltic Sea.

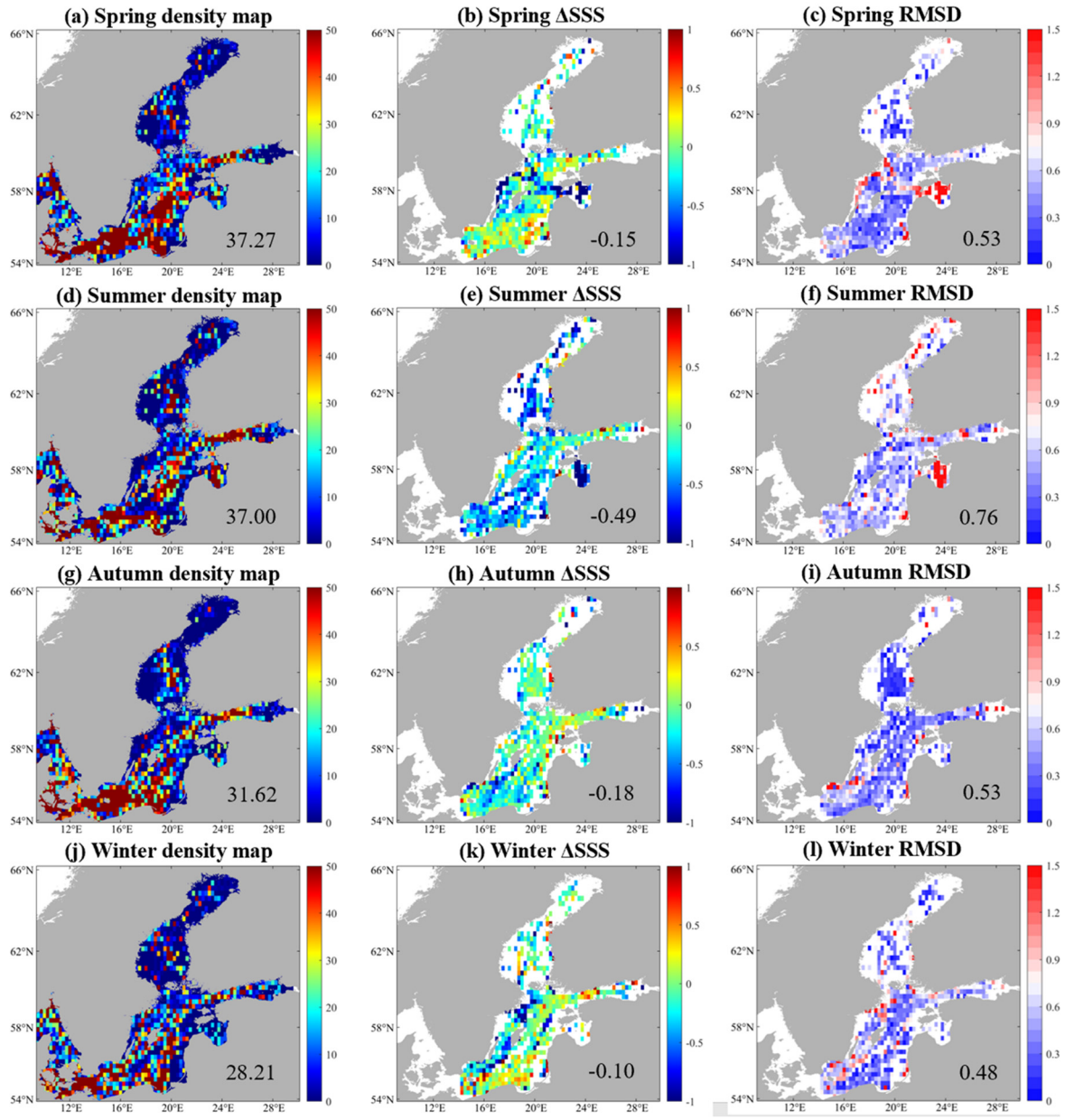


Figure 5. Spatial distribution of the data volume (**a,d,g,j**), mean ΔSSS values (**b,e,h,k**) and RMSDs (**c,f,i,l**) between the Baltic+SSS L4 data and collocated in situ SSS measurements. From top to bottom: Spring (March, April and May), Summer (June, July and August), Autumn (September, October and November) and Winter (December, January and February). The numbers labeled in the lowest right are the spatial average SSS (left), ΔSSS (middle) and RMSD (right) values. The unit is in PSU for ΔSSS and RMSD.

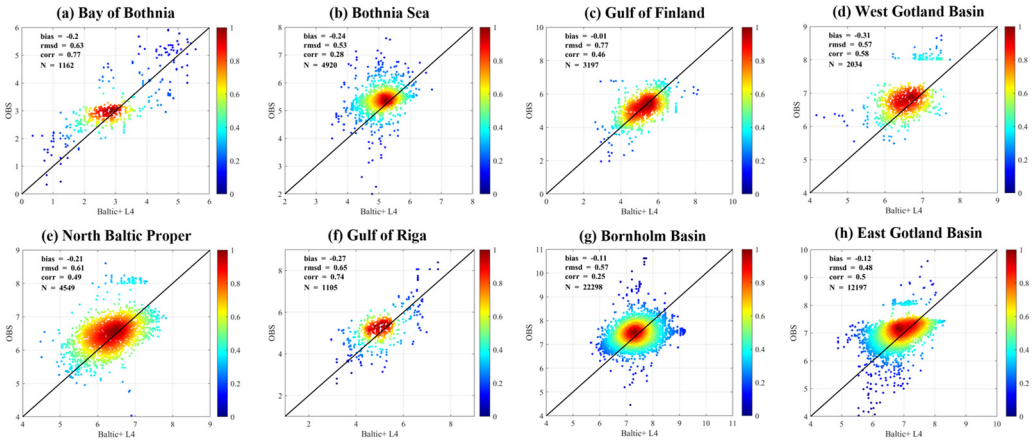


Figure 6. Density plot of 8-day SMOS BEC L4 versus collocated in situ SSS measurements for the eight zones of the Baltic Sea, including (**a**) the Bay of Bothnia, (**b**) the Bothnia Sea, (**c**) the Gulf of Finland, (**d**) the West Gotland Basin, (**e**) the North Baltic Proper, (**f**) the Gulf of Riga, (**g**) the Bornholm Basin, (**h**) the East Gotland Basin. The unit is in PSU for biases and RMSDs.

3.2. Global Comparison with In Situ Analyzed Products

Figure 7 presents the SSS maps in August 2017 from SMOS, SMAP, ISAS-20 and WODSSS gridded products. The reason for choosing the year 2017 was that El Niño and La Niña have less influence on the global climate. The spatial patterns of satellite and in situ analyzed SSS showed consistent large-scale spatial patterns, such as low salinities found in polar regions, the East Pacific Frehs Pool (EPFP) and the Eastern Indian Ocean; high salinities located in the subtropical north and south Atlantic; and extremely high salinity in the Mediterranean Sea. It is noteworthy that SMAP SSS appeared to depict more reasonable SSS structure than SMOS in areas close to land and the polar regions, such as the Mediterranean Sea, the East China Sea and the Chukchi Sea, which fills the gap between gridded SSS products from Aquarius and SMOS satellites. In this section, the comparison analysis of 57 months of SMOS BEC global L3 SSS (V2.0) was conducted at different space and time scales.

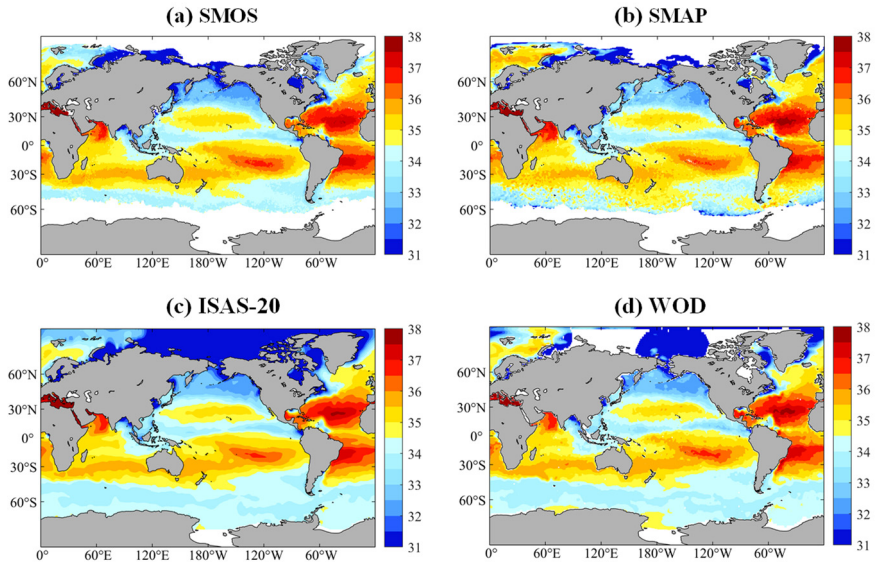


Figure 7. Global SSS maps for (**a**) Soil Moisture and Ocean Salinity (SMOS), (**b**) Soil Moisture Active-Passive (SMAP), (**c**) In Situ Analysis System (ISAS-20) and (**d**) WODSSS in August 2017. The unit is in the Practical Salinity Unit.

Figure 8 shows the global maps of mean ΔSSS, standard deviation, RMSD and correlation coefficient of SMOS with respect to the two OI in situ analyzed SSS products. In tropical to subtropical areas, the SMOS data show acceptable error away from the coast with the majority of ΔSSS values smaller than 0.1 PSU (–0.01 PSU on average) and correlation coefficients larger than 0.7 (passing the 95% significance test). Several regions with significant biases could be identified. Large ΔSSS values were found along the coastlines of almost each continent, which was most possibly caused by land contaminations, river discharge and Evaporation minus Precipitation (E-P), but part of the near-land errors can be originated from the under-sampling of drifting observation platforms. An example is the coast of South America near Chile, where the mean RMSD is nearly twice as large as the average STD. Large RMSD and low correlation coefficient occurring in the East/Japan Sea and Bay of Bengal are attributed to undetected RFI pollution. A wide range of fresher biases in the higher latitudes is partly caused by the reduced L-band radiometer sensitivity to salinity signals in cold water, whereas a worse performance of retrieval algorithm based solely on Brightness Temperature without corrections from radar wind and wave observations could also explain some part of errors. Additionally, areas with significant near-surface ocean stratification also contain large differences between SMOS and in situ measurements, such as the Eastern Pacific Fresh Pool (EPFP), where the correlation is significant with the p value smaller than 0.05 but the ΔSSS and RMSDs are too large. Finally, large RMSDs of SMOS are distributed near major river mouths (e.g., the Amazon River mouth region).

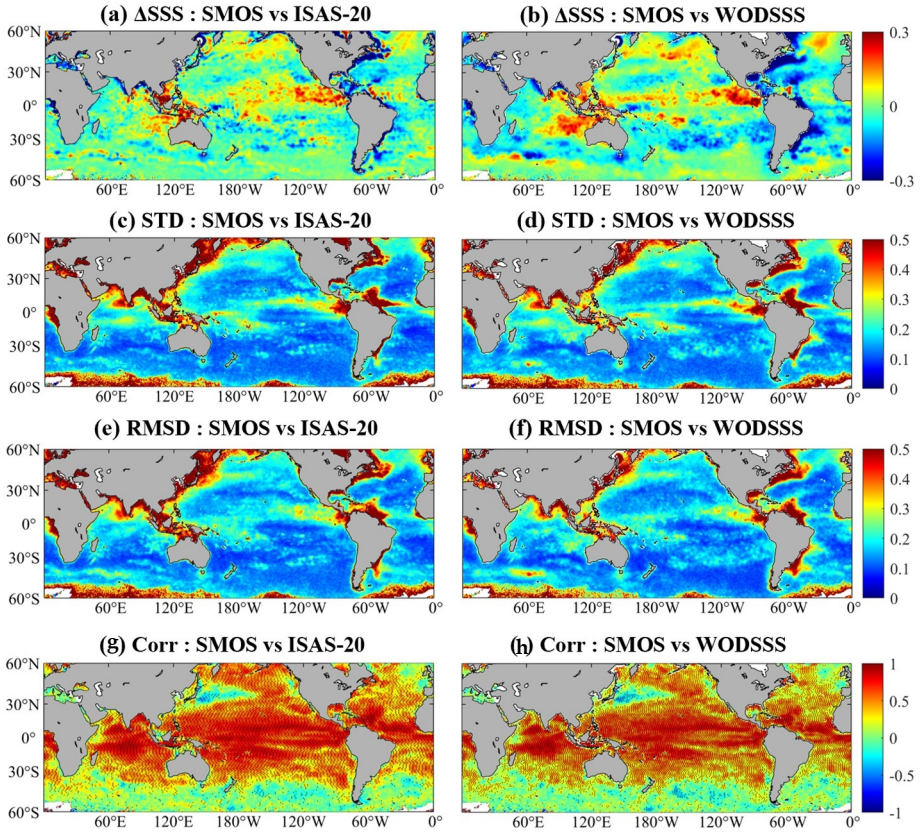


Figure 8. Comparison of Soil Moisture and Ocean Salinity (SMOS) SSS with (left) ISAS-20 and (right) WODSSS in terms of (**a,b**) ΔSSS, (**c,d**) STD, (**e,f**) RMSD and (**g,h**) correlation coefficient. Areas are specifically shaded where the correlation coefficients pass the 95% significance test with the corresponding p-values smaller than 0.05. The differences in time-mean SSS do not contribute to the STD values just as they do to the RMSD values.

Four types of regions were identified to carry large ΔSSS between SMOS and gridded in situ products:

(1) Polar regions where the sensitivity of the L-band radiometer decreases in cold water and brings negative SSS biases.
(2) Coastal areas where SSS data observed by drifting platforms are unreliable.
(3) Highly stratified seas where SMOS SSS differs from in situ measurements.
(4) Large river mouths influenced by the intrusion of fresh water.

After excluding the above areas with RMSD values larger than 0.4 PSU, we estimated the seasonal and interannual ΔSSS, RMSD and correlation coefficient in most open sea areas between 60°N and 60°S (Figure 9). Averaged over the rest of the regions, the ΔSSS between SMOS and in situ gridded data was close to zero with the mean RMSD and STD of ~0.2 PSU. Seasonal analysis showed that ΔSSS is more concentrated in winter months when the low average SST reduces the L-band radiometer sensitivity to salinity signals, which influences the ΔSSS values by ~0.05 PSU and RMSD values by ~0.02 PSU.

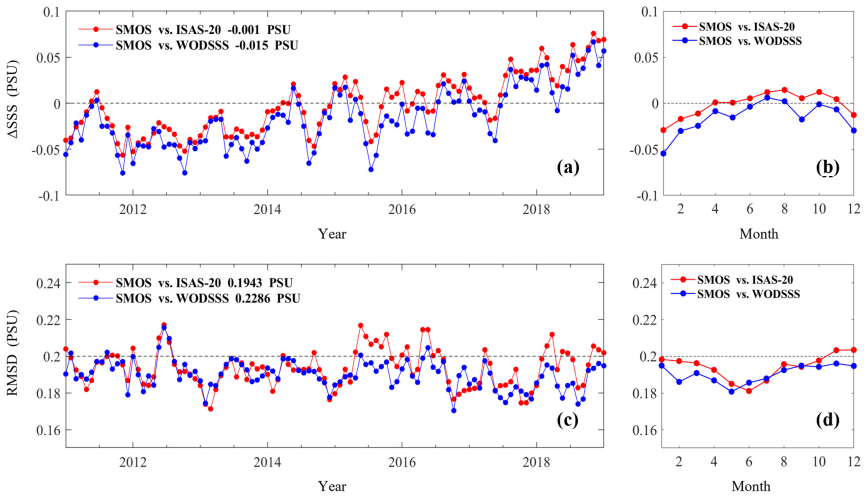


Figure 9. The long-term monthly (**a,c**) and seasonal (**b,d**) time series of ΔSSS (**a,b**) and RMSD (**c,d**) with respect to WODSSS and ISAS-20 data between 60°S and 60°N after excluding areas of excessive deviations.

It is also worth noting that both the comparison with WODSSS and ISAS-20 presents a phase shift of ΔSSS from negative to positive after 2014 and before 2018. By analyzing the mean ΔSSS field averaged in 2011–2015 and 2016–2019, respectively, we found the source of this ΔSSS increase signal is actually in the EPFP region of the equatorial Pacific Ocean (Figure S1). Further, based on the monthly OAFlux evaporation data and GPM precipitation data, we found a similar increasing trend of the Evaporation–Precipitation field near the EPFP region (Figure S4), which is mainly attributed to a decrease in rainfall rather than an increase in evaporation. A rain filter algorithm may be necessary to correct these positive errors of SMOS L3 product in the tropical Pacific Ocean.

Figure 10a shows the global average of the regional temporal RMSD between SMOS and two OI in situ analyzed SSS products for the spatial scales of 0.25° × 0.25°, 1° × 1°, 3° × 3° and 10° × 10°. The RMSD showed consistent values in SMOS with respect to both OI products, decreasing from ~0.27 PSU at 0.25° × 0.25° scale to ~0.19 PSU at 10° × 10° scale. This means that the SMOS SSS data showed smaller differences with in situ SSS data at larger spatial scales. The RMSD values were contributed by the differences in time-mean SSS values and differences in SSS anomalies (deviation from the time mean) between SMOS and in situ SSS. To separate the SSS differences contributed by the time-mean SSS values and SSS anomalies, we also examined the STD values between SMOS and in situ SSS. The differences in time-mean SSS did not contribute to the STD values just as they did to the RMSD values.

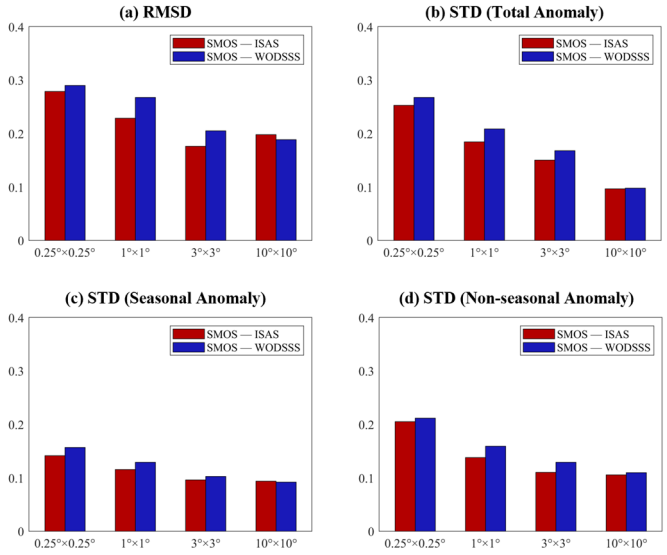


Figure 10. (**a**) Global average of temporal RMSD values between SMOS BEC L3 product and two in situ analyzed SSS products on four spatial scales indicated by legends along the horizontal axis. Global average of temporal STD values for the differences between SMOS BEC L3 product and two in situ analyzed SSS products on four different spatial scales for (**b**) total anomaly, (**c**) seasonal anomaly and (**d**) non-seasonal anomaly. RMSD and STD values are in the unit of PSU.

Figure 10b shows the global mean STD values of SSS differences between SMOS and two in situ analyzed SSS products at various spatial scales. The global average STD values for the 0.25° × 0.25°, 1° × 1°, 3° × 3° and 10° × 10° scales were 0.25, 0.18, 0.15 and 0.09 PSU for ISAS-20 and 0.26, 0.21, 0.16 and 0.09 PSU for WODSSS, respectively. Note that the RMSD and STD values with respect to in situ analyzed SSS not only contained the errors of the SMOS SSS, but also the errors of the gridded in situ SSS product. Figure 10c,d shows the global mean STD values for the components of seasonal anomalies and non-seasonal anomalies of SSS differences between SMOS and in situ analyzed SSS. It is noteworthy that the global average STD values for non-seasonal SSS anomalies was significantly larger than that for seasonal SSS anomalies under each spatial scale.

3.3. Comparison with Tropical Moored Buoys

Tropical moored buoys from the Global Tropical Moored Buoy Array (GTMBA) provide daily SSS measurements at fixed locations. These long-term daily sampling data are valuable for validation of SMOS data between the weekly scale and the interannual scale. The weekly time series of SMOS L3 product and in situ gridded SSS data at each buoy locations were selected using the nearest grid in the 0.25° × 0.25° boxes after applying a 7-day average filtering. As an example, Figure 11 shows the time series of 3 representative buoys in GTMBA arrays with more than 90 matched weekly samples. Results showed that SMOS and SMAP were consistent at weekly scales and provided salinity variations very similar to the buoys. It is noted that not only the flat trends correspond well, but also the rapid fluctuations of salinity at the buoy locations can be well captured by SMOS and SMAP data. A typical example was the rapid decrease of approximately 1.5 PSU occurring from 15 May 2018 at 4°N, 23°W. However, despite the fact that WODSSS and ISAS-20 data could generally corroborate the SMAP and SMOS SSS at monthly scale, they failed to catch the fluctuations with time scales shorter than 2 months limited by the time resolutions. Additionally, very small deviations were found between WODSSS and ISAS-20, which was attributed to the usage of similar OI algorithm and the abundant in situ observations merged into the models. The similarities between SMOS and tropical buoy SSS data proved that SMOS is capable of tracking salinity variations at weekly scale.

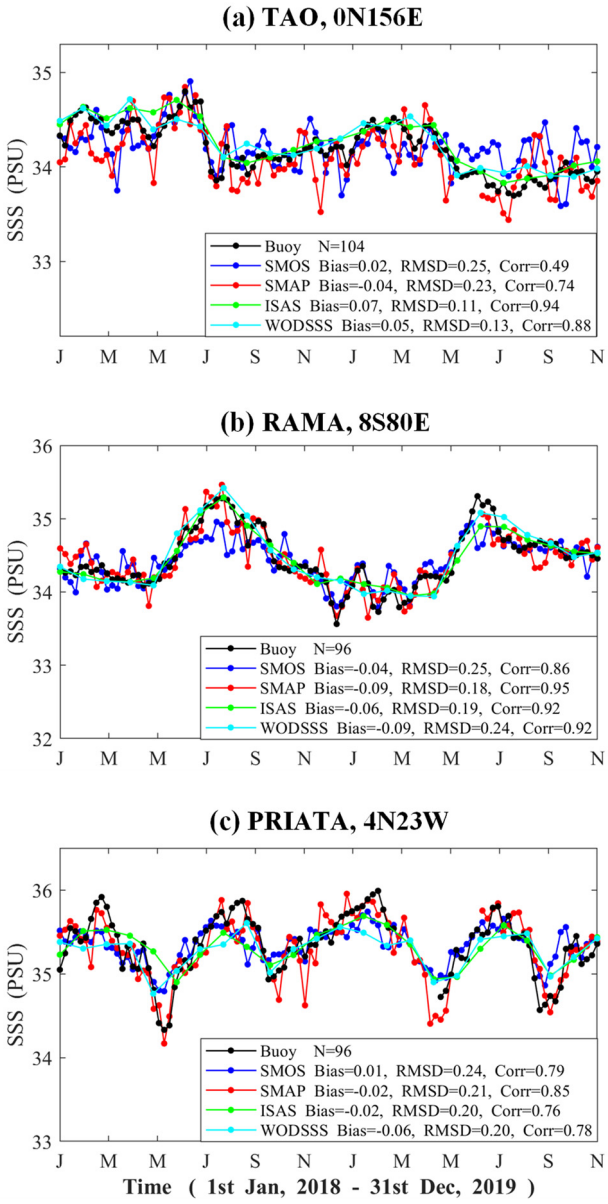


Figure 11. Time series of (**a**) buoy salinity at 1 m depth (black), collocated daily SMOS (blue) and 8-day SMAP (red), SSS plotted with monthly in situ data from WODSSS (azure) and ISAS-20 (green). Data are from (**a**) TAO at 0°N, 156°E, (**b**) RAMA at 8°S, 80°E, (**c**) PIRATA at 4°N, 23°W for the period from 1 January 2018 to 31 December 2019.

Figure 12 shows the comparison result of SMOS SSS with salinity from TAO in the Pacific Ocean, PIRATA in the Atlantic Ocean and RAMA in the Indian Ocean at weekly scale. We selected the time range of January 2018 to December 2019 because each buoy guaranteed more than 50 collocated weekly samples for comparison during this period. Generally, the SMOS SSS agreed well with the buoy arrays, with the correlation coefficient exceeding 0.6 in 55% of the TAO buoys, 64% of the PIRATA buoys and 78% of the RAMA buoys, all of which passed the significance test with p-values smaller than 0.05. Excluding buoys with significant errors (e.g., RAMA buoy at 15°N, 90°E), SMOS data showed negative ΔSSS at most sites, with the RMSDs no more than 0.3 PSU for most sites.

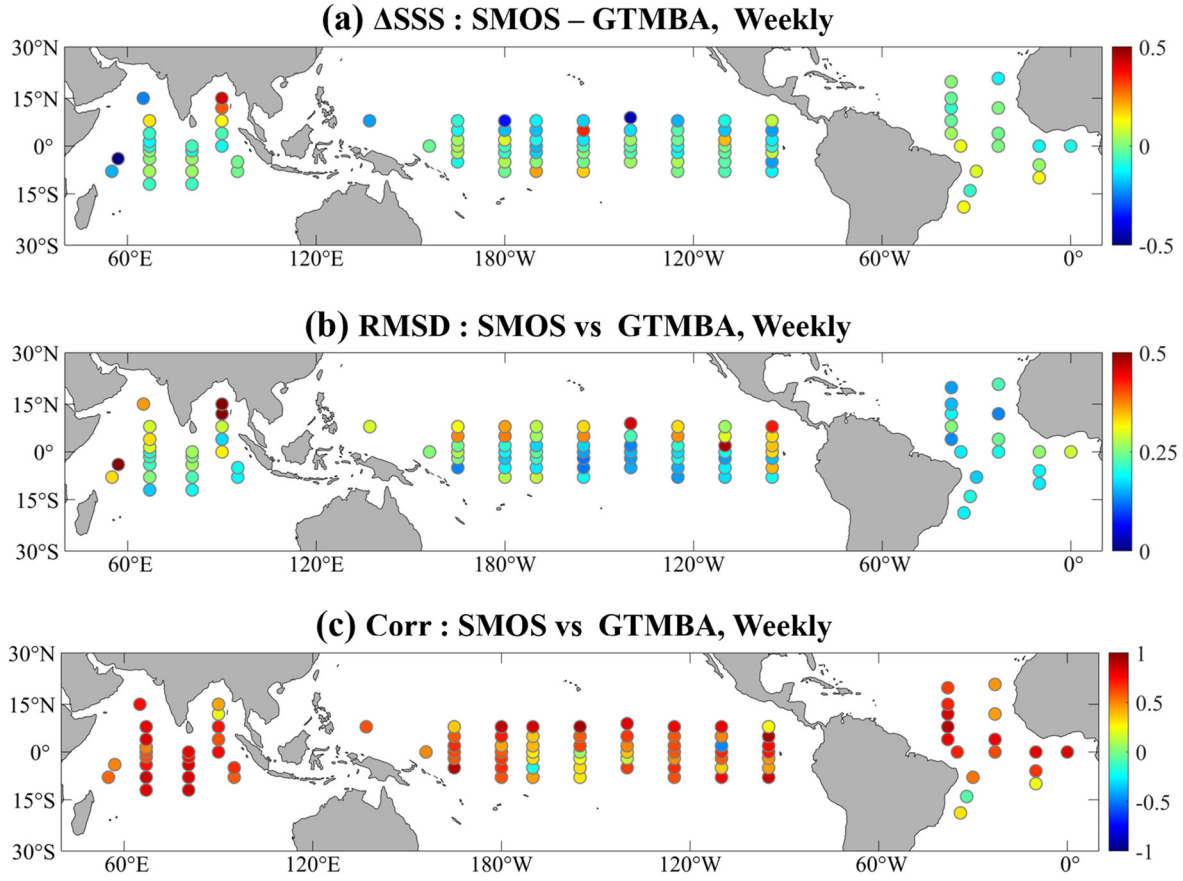


Figure 12. Comparison of SMOS SSS with salinity measured by GTMBA buoys at 1m depth at weekly scale in terms of (**a**) ΔSSS, (**b**) STD and (**c**) correlation coefficient. The time range was from 1 January 2018 to 31 December 2019.

Figure 13 shows the comparison results at the interannual scale using monthly SSS data from January 2011 to December 2019. The average seasonal variations were calculated and subtracted from the monthly time series at each annual cycle. Results showed that the SMOS had better agreement with buoys at the interannual scale compared with those at the weekly scale. The ΔSSS and RMSD values were generally smaller at most locations. The correlation coefficients exceeded 0.7 and passed the 95% significance test in 91% of the TAO buoys, 93% of the RAMA buoys and 82% of the PRIATA buoys. Buoys with significantly larger ΔSSS and RMSD values appeared at the same locations as those at the weekly scale, including the northern Bay of Bengal along 90°E influenced by river inflows, a few locations in the EPFP along 90°W influenced by heavy precipitation and several locations in the central Pacific influenced by strong ocean current.

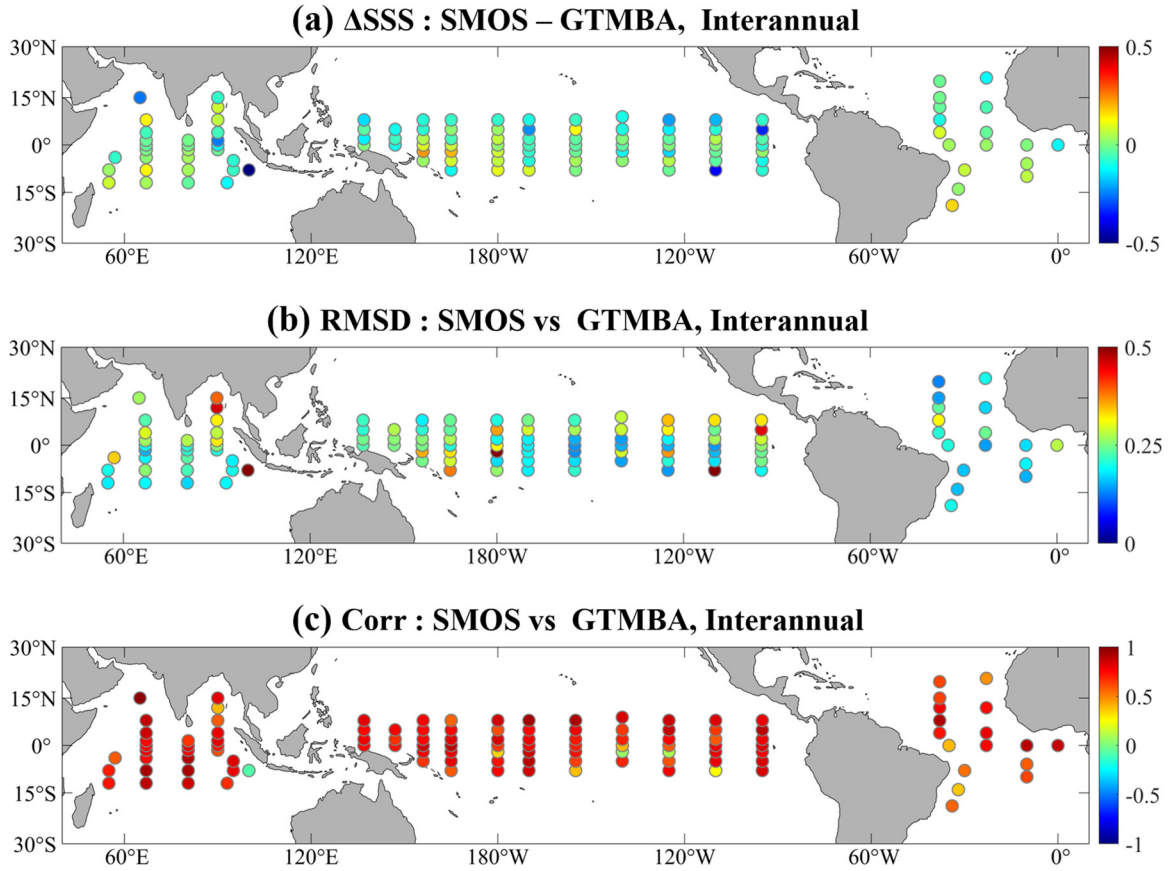


Figure 13. Comparison of SMOS SSS with salinity measured by GTMBA buoys at 1 m depth at interannual scale in terms of (**a**) ΔSSS, (**b**) STD and (**c**) correlation coefficient. The time range was from January 2011 to December 2019.

Figure 14 shows the histogram of ΔSSS and RMSD between satellite SSS and GTMBA buoy array data, which are generally consistent at weekly and interannual scales. The ΔSSS of SMOS and SMAP were mostly distributed between –0.2 to 0.2 PSU, which basically follows the Gaussian distribution at both scales. Compared with SMAP, SMOS had more positive ΔSSS with buoys, with a peak distribution of –0.1 PSU, which was consistent with the comparison result with both WOD and ISAS-20 in tropical regions. It is worth noting that our comparison results in 2018–2019 were contrary to those of [27], in which a comparison between SMOS and EN 4.2.1 showed negative ΔSSS in 2016–2017. This is likely attributed to the larger positive ΔSSS anomalies that appear in the equatorial Pacific Ocean, especially the Eastern Pacific Fresh Pool (EPFP) region. The distribution of RMSD between SMOS/SMAP and buoy data also conformed to the low RMSD in tropical seas (Figure 7c), and the mean RMSD of two satellites were equal.

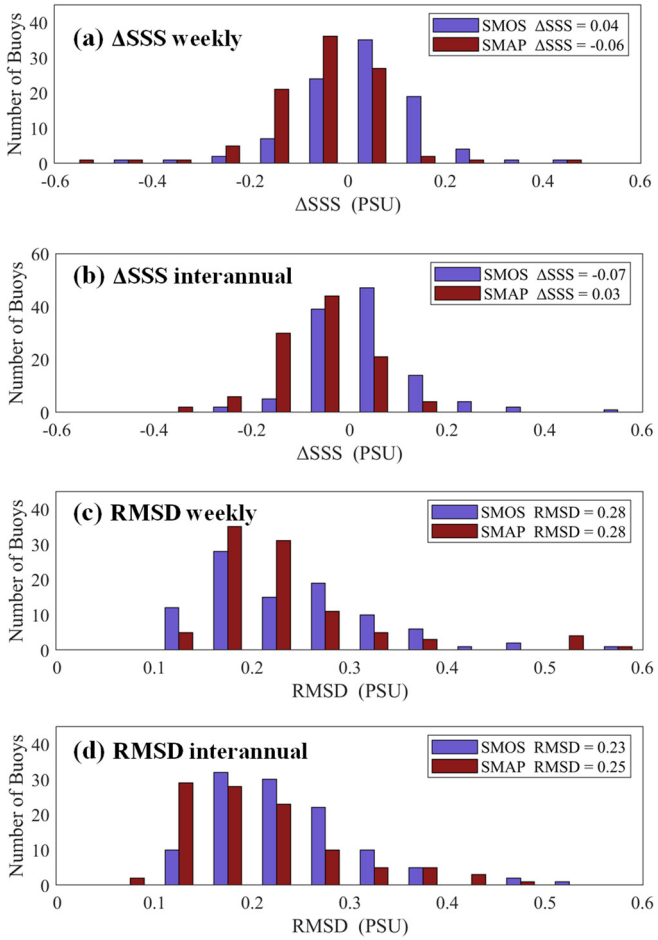


Figure 14. Histogram of ΔSSS and RMSD between SMOS BEC global L3 product (purple), SMAP JPL product (dark red), and GTMBA buoy salinity at 1 m. (**a**) Weekly ΔSSS, (**b**) interannual ΔSSS, (**c**) weekly RMSD, (**d**) interannual RMSD. The numbers in the top right legend are the corresponding average ΔSSS (**a**,**b**) and RMSD (**c**,**d**) values.

There are several buoys where we found large ΔSSS, RMSD and a low correlation coefficient with the collocated salinity data from both satellite and in situ products. Two typical examples are shown in Figure 15. For the TAO buoy located at 2°N, 125°E, the buoy salinity became progressively higher during November 2018 to February 2019, whereas the SMOS and SMAP SSS were in good agreement with each other and conformed to the collocated salinity data from WODSSS and ISAS-20. Another example is the PIRATA buoy at the location 21°N, 23°W, where the SSS value suddenly dropped by 0.5 PSU from June to July in the year of 2018 but the satellite SSS varied in a flat trend that coincided with the collocated salinity from WODSSS and ISAS-20. Given that the average value and the fundamental variation trend were not significantly different with satellite data, one probable explanation for the abnormal buoy data is a temporal malfunction of the mooring salinity sensor. This indicates that satellite data can be used to flag in situ observations for further consideration of possible instrument error after excluding all suspicious buoys with large drifts. However, this does not mean that buoy salinity cannot serve as ground truth since in most circumstances, the buoy SSS conformed to both the satellite SSS and the in situ analyzed SSS, and the large drifts contained in buoy SSS time series are significant enough and easy to be identified by a comparison with satellite SSS, as shown in the two samples given in Figure 15.

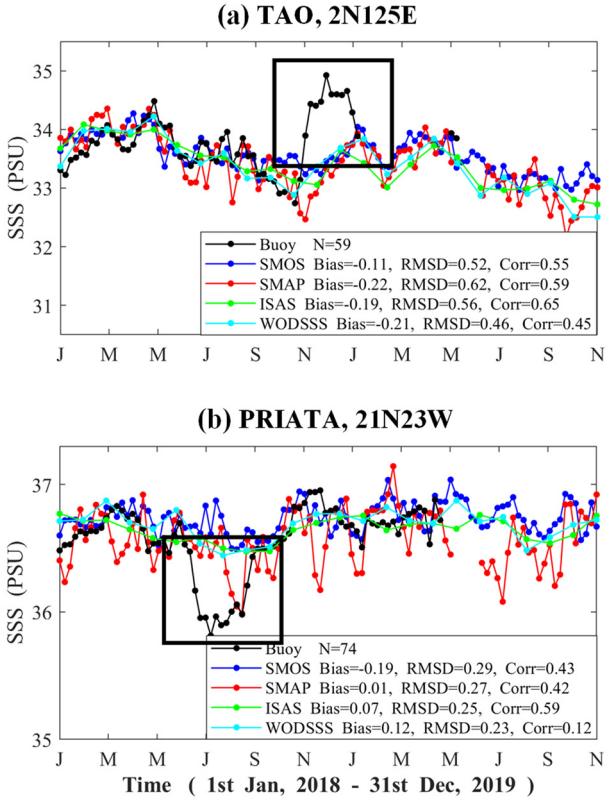


Figure 15. Time series of (**a**) problematic buoy salinity at 1 m depth (black), collocated daily SMOS (blue) and 8-day SMAP (red), SSS plotted with monthly in situ data from WODSSS (azure) and APDRC (blue). Data are from (left) TAO at 2°N, 125°E and (right) PIRATA at 21°N, 23°W.

4. Discussion

Compared to previous studies, the in situ measurements used in this study were much more extensive in space and longer in time, and the comparison was extended to more spatial and temporal scales than previous efforts. In situ data in other studies were primarily based on Argo profilers, which have a low spatial coverage in coastal areas and marginal seas, and can be supplied by the multi-source SSS measurements used in this study. By comparing with the newly updated ISAS-20 and WODSSS datasets, we found the RMSD values between satellite and in situ SSS are generally lower than 0.2 PSU and the mean ΔSSS value is lower than 0.05 PSU. In comparison [65] showed that the ΔSSS could reach as high as 0.1 PSU and [57] found the RMSD values were generally higher than 0.3 PSU.

The capacity of SMOS to retrieve salinity under extreme conditions was demonstrated by a multi-scale comparison in the Baltic Sea against the collocated GOSUD data along ship tracks, the WOD data collected from multiple in situ platforms and the BED stationary salinity data. We found a consistent spatial SSS structure between SMOS and in situ data with better performance away from the coast and river mouths. This is possibly due to the low sampling rates of in situ SSS measurements near the estuary and coastlines. Among three SMOS BEC products, the Baltic+SSS L4 product was closest to in situ measurements. Seasonal analysis showed that the influence of river discharge overrides the SST in producing SSS biases in the Baltic Sea. The comparison in eight subregions indicated that SMOS overestimated the SSS over the entire Baltic Sea. Among all subregions in the Baltic Sea, larger uncertainties were found in the Bay of Bothnia and the West Gotland Basin due to the under-sampling of in situ SSS measurements, and the largest SSS differences were found in the Gulf of Riga due to the dilution effect of river discharge and the contamination from land. The above results suggest that in such regions with a bad environment for SSS retrievals, despite the fact that the RFI and low SST correction algorithms have

been developed and used in both SMOS and in situ analyzed products, some physical or empirical methods are still required for SSS correction in areas influenced by river inflow, precipitation and evaporation. Our study also suggests the difficulty of validating satellite SSS at high spatiotemporal scales in marginal seas, given the paucity of in situ SSS measurements in semi-closed regions where Argo profiles are not sufficient. Perfection of the in situ observing system is crucial for the improvement of satellite SSS data quality in marginal seas and coastal regions, which is beneficial to support dynamic studies on the mesoscale salinity features and cross-basin ocean fronts.

By comparing with in situ analyzed SSS data from WODSSS and ISAS-20, we concluded that the SSS retrieved from SMOS L-band radiometer presented the mean bias of 0.2 PSU in open seas between 60°N and 60°S. Several regions with large discrepancies between SMOS and in situ SSS measurements were identified, suggesting the need for an improved SSS retrieval algorithm in the future to eliminate SSS errors in cold water, coastal areas, large river mouths and highly stratified seas. As the spatial scale increased, the uncertainty of SSS decreased, with the smallest ΔSSS and RMSD values seen at $0.25^\circ \times 0.25^\circ$ scale. Additionally, we found the mean ΔSSS between SMOS and in situ salinity (excluding polar regions) has increased from negative to positive since 2016, which is related to decreased rainfall in the tropical Pacific Ocean. Moreover, it is worth noting that the RMSD, STD and ΔSSS values reported in this study were not solely attributed to the SSS uncertainties in satellite products. The insufficient data sampling rates also contributed to some of the large discrepancies between SMOS and in situ SSS. The SSS data retrieved from L-band satellite radiometer represents the mean SSS value along the footprints, which has a range of about 40 km for SMOS. In contrast, the in situ SSS is generally point-wise and represents the average values over a far smaller area than satellite footprints. This difference can be significant enough in seawater with strong gradients, such as in the river mouths, ocean fronts and mesoscale eddies. Furthermore, it is expected that the SSS measurements by both the in situ platforms and satellite missions could possibly figure out whether the phase shift of ΔSSS in equatorial Pacific Ocean ultimately resulted from data error, regional variabilities or climate change.

The comparison of collocated SSS time series from SMOS, SMAP and mooring buoy data showed that SMOS could accurately capture the SSS variations at weekly and interannual scales. Similar to the global comparison with in situ analyzed products, the regional comparison with GTMBA buoys also indicates that statistical differences between satellite and buoy SSS data do not only reflect the uncertainties of remote sensing but also the malfunction of sensors installed on the in situ platforms. Based on the demonstration of consistency and discrepancy among SSS data from SMOS, buoy and in situ analyzed products, we concluded that satellite SSS has the potential to validate and serve as the real-time quality control (QC) of buoy salinity data at a weekly scale. Moreover, it can be further induced that satellite SSS is potentially useful in correcting the SSS data observed by Argo profilers, but a higher resolution version of the satellite SSS product is expected to achieve this function.

5. Conclusions

In this study, the SMOS SSS retrieved from brightness temperature data at BEC was compared with in situ salinity measurements from analyzed products, tropical mooring buoys and ocean observation databases at different time and space scales.

Compared with collocated in situ SSS measurements provided by various observation platforms, the spatial SSS structure of SMOS was consistent with in situ measurements, with relatively worse performance near the coastlines and river mouths. Among three SMOS BEC products, the Baltic+SSS L4 product had the highest data quality in the Baltic Sea. The comparative analysis at different seasons indicates that the SSS biases are larger in summer than in other seasons, suggesting the river runoff may override the SST in determining the SSS retrieval performance of the SMOS satellite in the Baltic Sea. An assessment of different regions showed that large biases appear in regions near the coast

and river mouths, such as the Bay of Bothnia, the Bothnia Sea and the West Gotland Basin, where sparse in situ measurements also contributed to part of the SSS biases. This indicates that additional ship surveys should be conducted over these subregions to achieve a more refined comparison and validation.

By comparing with in situ analyzed SSS data from WODSSS and ISAS-20, we concluded that the SSS retrieved from the SMOS L-band radiometer presented the mean bias of 0.2 PSU in open seas between 60°N and 60°S. Several regions with large discrepancies between SMOS and in situ SSS measurements were identified, suggesting the need for an improved SSS retrieval algorithm in the future to eliminate SSS errors in cold water, coastal areas, large river mouths and highly stratified seas. As the spatial scale increased, the uncertainty of SSS decreased, with the smallest ΔSSS and RMSD values seen at 0.25° × 0.25° scale. Additionally, we found the mean ΔSSS between SMOS and in situ salinity (excluding polar regions) has increased from negative to positive since 2016, which is related to decreased rainfall in the tropical Pacific Ocean.

The comparison SSS from the collocated SMOS, SMAP and mooring buoy data showed that SMOS could accurately capture the SSS variations at both the weekly and interannual scales, similar to the global comparison with in situ analyzed products. The consistency and discrepancy among satellite, buoy and in situ analyzed SSS indicate that SMOS salinity has the potential to serve as the real-time quality control (QC) of buoy salinity at a weekly scale.

Finally, new versions of the satellite SSS product with longer time series, higher spatiotemporal resolution and improved retrieval method will be developed by various institutions in the future, such as the Barcelona Expert Center (BEC) and the Centre Aval de Traitement des Données SMOS (CATDS). We will be able to analyze salinity changes at global scale with increased temporal/spatial resolution and get a better understanding of their underlying link to the global hydrological cycle and climate change.

Supplementary Materials: The following are available online at https://www.mdpi.com/article/10.3390/rs14215465/s1, Figure S1: ΔSSS of Sea Surface Salinity (SSS) averaged from (a) April 2011 to January 2016 and (b) February 2016 to December 2019, Figure S2: Precipitation rate averaged from (a) April 2011 to January 2016 and (b) February 2016 to December 2019. The unit is mm/hour, Figure S3: Evaporation rate averaged from (a) April 2011 to January 2016 and (b) February 2016 to December 2019. The unit is mm/hour, Figure S4: The rate of evaporation minus precipitation averaged from (a) April 2011 to January 2016 and (b) February 2016 to December 2019. The unit is mm/hour. Figure S5: Seasonal freshwater discharge from 256 rivers flowing into the Baltic Sea based on Global Data Runoff Center (GRDC) Data.

Author Contributions: All the authors played a critical part in the preparation of the manuscript. Conceptualization, H.W.; methodology, H.W.; software, H.W. and K.R.; validation, H.W., S.B., W.C. and K.R.; formal analysis, H.W. and S.B.; investigation, H.W. and S.B.; resources, H.W. and K.R.; data curation, H.W., S.B., W.C and K.H.; writing—original draft preparation, H.W.; writing—review and editing, H.W.; visualization, S.B.; supervision, K.R.; project administration, K.R.; funding acquisition, K.H. All authors have read and agreed to the published version of the manuscript.

Funding: The research described in this paper was carried out in the College of Meteorology and Oceanography, National University of Defense Technology. This work was supported by the National Natural Science Foundation of China under Grant No. 61901488.

Data Availability Statement: All SSS data presented in this study are openly and freely available. The WOA18 and WOD monthly salinity anomaly data are available from the National Centers for Environmental Information (NCEI) and can be accessed at https://www.ncei.noaa.gov/access/world-ocean-atlas-2018/bin/woa18.pl?parameter=s and https://www.ncei.noaa.gov/access/global-ocean-heat-content/bin/anomalydata_sm.pl. The ISAS-20 data are available from https://www.seanoe.org/data/00412/52367/. The SMOS L3 product was provided by the http://bec.icm.csic.es/ (BEC) and is available at sftp://becftp.icm.csic.es:27500. The 8-day running mean SMAP RSS product is available at https://podaac.jpl.nasa.gov/dataset/SMAP_RSS_L3_SSS_SMI_8DAY-RUNNINGMEAN_V4. The daily-averaged mooring buoy data are freely accessible at www.pmel.noaa.gov/tao. The volunteer ship data provided by Global Ocean Surface Underway Data (GOSUD) can be downloaded from ftp://ftp.ifremer.fr/ifremer/gosudv3/latest. Salinity data used for evaluation in the Baltic Sea were

extracted from the Baltic Environmental Database (BED, http://nest.su.se/bed) at Stockholm University. The Global Data Runoff Center (GRDC) data are accessible from https://portal.grdc.bafg.de/.

Acknowledgments: We appreciate access to all the freely available products that made this study possible. These products include gridded salinity products from EN4, JASMTEC, IAP, IPRC, SIO and BOA. The satellite SSS data include products released by the LOCEAN/IPSL (UMR CNRS/UPMC/IRD/MNHN) laboratory and ACRI-st company, the Barcelona Expert Center, the ESA climate office and the E.U. Copernicus Marine Service Information.

Conflicts of Interest: The authors declare no conflict of interest.

References

1. Plummer, S.; Lecomte, P.; Doherty, M. The ESA Climate Change Initiative (CCI): A European contribution to the generation of the Global Climate Observing System. *Remote Sens. Environ.* **2017**, *203*, 2–8. [CrossRef]
2. Skliris, N.; Marsh, R.; Josey, S.A.; Good, S.A.; Liu, C.; Allan, R.P. Salinity changes in the World Ocean since 1950 in relation to changing surface freshwater fluxes. *Clim. Dyn.* **2014**, *43*, 709–736. [CrossRef]
3. Matthäus, W.; Schinke, H. The influence of river runoff on deep water conditions of the Baltic Sea. In *Biological, Physical and Geochemical Features of Enclosed and Semi-Enclosed Marine Systems*; Springer: Berlin/Heidelberg, Germany, 1999; pp. 1–10.
4. Durack, P.J.; Wijffels, S.E.; Matear, R.J. Ocean salinities reveal strong global water cycle intensification during 1950 to 2000. *Science* **2012**, *336*, 455–458. [CrossRef]
5. Yu, L.; Josey, S.A.; Bingham, F.M.; Lee, T. Intensification of the global water cycle and evidence from ocean salinity: A synthesis review. *Ann. N. Y. Acad. Sci.* **2020**, *1472*, 76–94. [CrossRef] [PubMed]
6. Johnson, H.L.; Cessi, P.; Marshall, D.P.; Schloesser, F.; Spall, M.A. Recent Contributions of Theory to Our Understanding of the Atlantic Meridional Overturning Circulation. *J. Geophys. Res. Ocean.* **2019**, *124*, 5376–5399. [CrossRef]
7. Johnson, G.C.; Schmidtko, S.; Lyman, J.M. Relative contributions of temperature and salinity to seasonal mixed layer density changes and horizontal density gradients. *J. Geophys. Res. Ocean.* **2012**, *117*, C4. [CrossRef]
8. Du, Y.; Zhang, Y.; Shi, J. Relationship between sea surface salinity and ocean circulation and climate change. *Sci. China Earth Sci.* **2019**, *62*, 771–782. [CrossRef]
9. Hsu, P.-C.; Centurioni, L.; Shao, H.-J.; Zheng, Q.; Lu, C.-Y.; Hsu, T.-W.; Tseng, R.-S. Surface Current Variations and Oceanic Fronts in the Southern East China Sea: Drifter Experiments, Coastal Radar Applications, and Satellite Observations. *J. Geophys. Res. Ocean.* **2021**, *126*, e2021JC017373. [CrossRef]
10. D'Addezio, J.M.; Subrahmanyam, B. Sea surface salinity variability in the Agulhas Current region inferred from SMOS and Aquarius. *Remote Sens. Environ.* **2016**, *180*, 440–452. [CrossRef]
11. Hasson, A.; Farrar, J.T.; Boutin, J.; Bingham, F.; Lee, T. Intraseasonal Variability of Surface Salinity in the Eastern Tropical Pacific Associated With Mesoscale Eddies. *J. Geophys. Res. Ocean.* **2019**, *124*, 2861–2875. [CrossRef]
12. Melnichenko, O.; Hacker, P.; Müller, V. Mesoscale eddies in satellite sea surface salinity data and inferred eddy freshwater transports. In *Geophysical Research Abstracts*; European Geosciences Union: Amsterdam, Netherlands, 2019; Volume 21.
13. Kerr, Y.H.; Waldteufel, P.; Wigneron, J.; Delwart, S.; Cabot, F.; Boutin, J.; Escorihuela, M.; Font, J.; Reul, N.; Gruhier, C.; et al. The SMOS Mission: New Tool for Monitoring Key Elements ofthe Global Water Cycle. *Proc. IEEE* **2010**, *98*, 666–687. [CrossRef]
14. Font, J.; Camps, A.; Borges, A.; Martín-Neira, M.; Boutin, J.; Reul, N.; Kerr, Y.H.; Hahne, A.; Mecklenburg, S. SMOS: The Challenging Sea Surface Salinity Measurement From Space. *Proc. IEEE* **2010**, *98*, 649–665. [CrossRef]
15. Vine, D.M.L.; Lagerloef, G.S.E.; Colomb, F.R.; Yueh, S.H.; Pellerano, F.A. Aquarius: An Instrument to Monitor Sea Surface Salinity From Space. *IEEE Trans. Geosci. Remote Sens.* **2007**, *45*, 2040–2050. [CrossRef]
16. Entekhabi, D.; Njoku, E.; Neill, P.O.; Spencer, M.; Jackson, T.; Entin, J.; Im, E.; Kellogg, K. The Soil Moisture Active/Passive Mission (SMAP). In Proceedings of the IGARSS 2008—2008 IEEE International Geoscience and Remote Sensing Symposium, Boston, MA, USA, 7–11 July 2008; pp. III-1–III-4.
17. Zine, S.; Boutin, J.; Font, J.; Reul, N.; Waldteufel, P.; Gabarro, C.; Tenerelli, J.; Petitcolin, F.; Vergely, J.L.; Talone, M.; et al. Overview of the SMOS Sea Surface Salinity Prototype Processor. *IEEE Trans. Geosci. Remote Sens.* **2008**, *46*, 621–645. [CrossRef]
18. Lagerloef, G.; Colomb, F.R.; Le Vine, D.; Wentz, F.; Yueh, S.; Ruf, C.; Lilly, J.; Gunn, J.; Chao, Y.; Decharon, A. The Aquarius/SAC-D mission: Designed to meet the salinity remote-sensing challenge. *Oceanography* **2008**, *21*, 68–81. [CrossRef]
19. Reul, N.; Tenerelli, J.; Chapron, B.; Vandemark, D.; Quilfen, Y.; Kerr, Y. SMOS satellite L-band radiometer: A new capability for ocean surface remote sensing in hurricanes. *J. Geophys. Res. Ocean.* **2012**, *117*. [CrossRef]
20. Misra, S.; Piepmeier, J.R.; Peng, J.; Mohammed, P.N.; Hudson, D.; Amici, G.D.; Dinnat, E.; Vine, D.L.; Bindlish, R.; Jackson, T. Calibration and validation of the SMAP L-band radiometer. In Proceedings of the 2016 IEEE International Geoscience and Remote Sensing Symposium (IGARSS), Beijing, China, 10–15 July 2016; pp. 120–122.
21. Piepmeier, J.R.; Levine, D.M.; Yueh, S.H.; Wentz, F.; Ruf, C. Aquarius radiometer performance: Early on-orbit calibration and results. In Proceedings of the International Geoscience and Remote Sensing Symposium (IGARSS), Munich, Germany, 22 July 2012.
22. Park, H.; González-Gambau, V.; Camps, A.; Vall-llossera, M. Improved MUSIC-Based SMOS RFI Source Detection and Geolocation Algorithm. *IEEE Trans. Geosci. Remote Sens.* **2016**, *54*, 1311–1322. [CrossRef]

23. Boutin, J.; Vergely, J.-L.; Marchand, S.; d'Amico, F.; Hasson, A.; Kolodziejczyk, N.; Reul, N.; Reverdin, G.; Vialard, J. New SMOS Sea Surface Salinity with reduced systematic errors and improved variability. *Remote Sens. Environ.* **2018**, *214*, 115–134. [CrossRef]
24. Kolodziejczyk, N.; Boutin, J.; Vergely, J.-L.; Marchand, S.; Martin, N.; Reverdin, G. Mitigation of systematic errors in SMOS sea surface salinity. *Remote Sens. Environ.* **2016**, *180*, 164–177. [CrossRef]
25. Corbella, I.; Durán, I.; Lin, W.; Torres, F.; Duffo, N.; Khazâal, A.; Martín-Neira, M. Mitigation of land-sea contamination in SMOS. In Proceedings of the 2015 IEEE International Geoscience and Remote Sensing Symposium (IGARSS), Milan, Italy, 26–31 July 2015; pp. 1433–1436.
26. Olmedo, E.; Martínez, J.; Turiel, A.; Ballabrera-Poy, J.; Portabella, M. Debiased non-Bayesian retrieval: A novel approach to SMOS Sea Surface Salinity. *Remote Sens. Environ.* **2017**, *193*, 103–126. [CrossRef]
27. Bao, S.; Wang, H.; Zhang, R.; Yan, H.; Chen, J. Comparison of Satellite-Derived Sea Surface Salinity Products from SMOS, Aquarius, and SMAP. *J. Geophys. Res. Ocean.* **2019**, *124*, 1932–1944. [CrossRef]
28. Xie, J.; Raj, R.P.; Bertino, L.; Samuelsen, A.; Wakamatsu, T. Evaluation of Arctic Ocean surface salinities from the Soil Moisture and Ocean Salinity (SMOS) mission against a regional reanalysis and in situ data. *Ocean. Sci.* **2019**, *15*, 1191–1206. [CrossRef]
29. Yi, D.L.; Melnichenko, O.; Hacker, P.; Potemra, J. Remote sensing of sea surface salinity variability in the South China Sea. *J. Geophys. Res. Ocean.* **2020**, *125*, e2020JC016827. [CrossRef]
30. Roemmich, D.; Johnson, G.C.; Riser, S.; Davis, R.; Gilson, J.; Owens, W.B.; Garzoli, S.L.; Schmid, C.; Ignaszewski, M. The Argo Program: Observing the Global Ocean with Profiling Floats. *Oceanography* **2009**, *22*, 34–43. [CrossRef]
31. Menezes, V.V. Statistical assessment of sea-surface salinity from SMAP: Arabian Sea, Bay of Bengal and a promising Red Sea application. *Remote Sens.* **2020**, *12*, 447. [CrossRef]
32. Olmedo, E.; Gabarró, C.; González-Gambau, V.; Martínez, J.; Ballabrera-Poy, J.; Turiel, A.; Portabella, M.; Fournier, S.; Lee, T. Seven years of SMOS sea surface salinity at high latitudes: Variability in Arctic and Sub-Arctic regions. *Remote Sens.* **2018**, *10*, 1772. [CrossRef]
33. Abe, H.; Ebuchi, N. Evaluation of sea-surface salinity observed by A quarius. *J. Geophys. Res. Ocean.* **2014**, *119*, 8109–8121. [CrossRef]
34. Grodsky, S.A.; Vandemark, D.; Feng, H. Assessing coastal SMAP surface salinity accuracy and its application to monitoring Gulf of Maine circulation dynamics. *Remote Sens.* **2018**, *10*, 1232. [CrossRef]
35. Fournier, S.; Lee, T.; Tang, W.; Steele, M.; Olmedo, E. Evaluation and intercomparison of SMOS, Aquarius, and SMAP sea surface salinity products in the Arctic Ocean. *Remote Sens.* **2019**, *11*, 3043. [CrossRef]
36. Garcia-Eidell, C.; Comiso, J.C.; Dinnat, E.; Brucker, L. Satellite observed salinity distributions at high latitudes in the N orthern H emisphere: A comparison of four products. *J. Geophys. Res. Ocean.* **2017**, *122*, 7717–7736. [CrossRef]
37. Bingham, F.M.; Brodnitz, S.; Yu, L. Sea surface salinity seasonal variability in the tropics from satellites, gridded in situ products and mooring observations. *Remote Sens.* **2020**, *13*, 110. [CrossRef]
38. Tang, W.; Yueh, S.H.; Fore, A.G.; Hayashi, A. Validation of A quarius sea surface salinity with in situ measurements from A rgo floats and moored buoys. *J. Geophys. Res. Ocean.* **2014**, *119*, 6171–6189. [CrossRef]
39. Yu, L. Variability and uncertainty of satellite sea surface salinity in the subpolar North Atlantic (2010–2019). *Remote Sens.* **2020**, *12*, 2092. [CrossRef]
40. Zhao, J.; Wang, Y.; Liu, W.; Bi, H.; Cokelet, E.D.; Mordy, C.W.; Lawrence-Slavas, N.; Meinig, C. Sea Surface Salinity Variability in the Bering Sea in 2015–2020. *Remote Sens.* **2022**, *14*, 758. [CrossRef]
41. Martins, M.S.; Stammer, D. Interannual Variability of the Congo River Plume-Induced Sea Surface Salinity. *Remote Sens.* **2022**, *14*, 1013. [CrossRef]
42. Vazquez-Cuervo, J.; Fournier, S.; Dzwonkowski, B.; Reager, J. Intercomparison of In-Situ and Remote Sensing Salinity Products in the Gulf of Mexico, a River-Influenced System. *Remote Sens.* **2018**, *10*, 1590. [CrossRef]
43. Ferster, B.S.; Subrahmanyam, B. A Comparison of Satellite-Derived Sea Surface Salinity and Salt Fluxes in the Southern Ocean. *Remote Sens. Earth Syst. Sci.* **2018**, *1*, 1–13. [CrossRef]
44. Lee, T. Consistency of Aquarius sea surface salinity with Argo products on various spatial and temporal scales. *Geophys. Res. Lett.* **2016**, *43*, 3857–3864. [CrossRef]
45. Dinnat, E.P.; Le Vine, D.M.; Boutin, J.; Meissner, T.; Lagerloef, G. Remote sensing of sea surface salinity: Comparison of satellite and in situ observations and impact of retrieval parameters. *Remote Sens.* **2019**, *11*, 750. [CrossRef]
46. Wang, J.; Sun, W.; Zhang, J. Sea surface salinity products validation based on triple match method. *IEEE J. Sel. Top. Appl. Earth Obs. Remote Sens.* **2019**, *12*, 4361–4366. [CrossRef]
47. González-Gambau, V.; Olmedo, E.; Turiel, A.; González-Haro, C.; García-Espriu, A.; Martínez, J.; Alenius, P.; Tuomi, L.; Catany, R.; Arias, M. First SMOS Sea Surface Salinity dedicated products over the Baltic Sea. *Earth Syst. Sci. Data* **2022**, *14*, 2343–2368. [CrossRef]
48. Vazquez-Cuervo, J.; Gomez-Valdes, J.; Bouali, M.; Miranda, L.E.; Van der Stocken, T.; Tang, W.; Gentemann, C. Using saildrones to validate satellite-derived sea surface salinity and sea surface temperature along the California/Baja Coast. *Remote Sens.* **2019**, *11*, 1964. [CrossRef]
49. Fournier, S.; Lee, T.; Gierach, M.M. Seasonal and interannual variations of sea surface salinity associated with the Mississippi River plume observed by SMOS and Aquarius. *Remote Sens. Environ.* **2016**, *180*, 431–439. [CrossRef]

50. Hall, S.B.; Subrahmanyam, B.; Morison, J.H. Intercomparison of Salinity Products in the Beaufort Gyre and Arctic Ocean. *Remote Sens.* **2021**, *14*, 71. [CrossRef]
51. Kerr, Y.H.; Waldteufel, P.; Wigneron, J.-P.; Martinuzzi, J.; Font, J.; Berger, M. Soil moisture retrieval from space: The Soil Moisture and Ocean Salinity (SMOS) mission. *IEEE Trans. Geosci. Remote Sens.* **2001**, *39*, 1729–1735. [CrossRef]
52. Olmedo, E.; González-Haro, C.; González Gambau, V.; Martínez, J.; Turiel, A. *Global SMOS-BEC SSS L3 and L4 Product v2 Description*; CSIC/Barcelona Expert Center: Barcelona, Spain, 2020.
53. Meissner, T.; Wentz, F.J.; Le Vine, D.M. The Salinity Retrieval Algorithms for the NASA Aquarius Version 5 and SMAP Version 3 Releases. *Remote Sens.* **2018**, *10*, 1121. [CrossRef]
54. Fore, A.G.; Yueh, S.H.; Tang, W.; Stiles, B.W.; Hayashi, A.K. Combined Active/Passive Retrievals of Ocean Vector Wind and Sea Surface Salinity With SMAP. *IEEE Trans. Geosci. Remote Sens.* **2016**, *54*, 7396–7404. [CrossRef]
55. Gaillard, F.; Reynaud, T.; Thierry, V.; Kolodziejczyk, N.; von Schuckmann, K. In Situ–Based Reanalysis of the Global Ocean Temperature and Salinity with ISAS: Variability of the Heat Content and Steric Height. *J. Clim.* **2016**, *29*, 1305–1323. [CrossRef]
56. Kolodziejczyk, N.; Prigent-Mazella, A.; Gaillard, F. *ISAS Temperature and Salinity Gridded Fields*; SEANOE: Plouzané, France, 2021. [CrossRef]
57. Zweng, M.; Reagan, J.; Seidov, D.; Boyer, T.; Locarnini, M.; Garcia, H.; Mishonov, A.; Baranova, O.; Weathers, K.; Paver, C.; et al. World Ocean Atlas 2018, Volume 2: Salinity. NOAA Atlas NESDIS: Silverspring, MD, USA, 2019; Volume 82, p. 50.
58. Reagan, J.; Boyer, T.; Antonov, J.; Zweng, M. Comparison analysis between Aquarius sea surface salinity and World Ocean D atabase in situ analyzed sea surface salinity. *J. Geophys. Res. Ocean.* **2014**, *119*, 8122–8140. [CrossRef]
59. Köhler, J.; Sena Martins, M.; Serra, N.; Stammer, D. Quality assessment of spaceborne sea surface salinity observations over the northern North Atlantic. *J. Geophys. Res. Ocean.* **2015**, *120*, 94–112. [CrossRef]
60. McPhaden, M.J. The Tropical Atmosphere Ocean Array Is Completed. *Bull. Am. Meteorol. Soc.* **1995**, *76*, 739–741. [CrossRef]
61. Servain, J.; Busalacchi, A.J.; McPhaden, M.J.; Moura, A.D.; Reverdin, G.; Vianna, M.; Zebiak, S.E. A pilot research moored array in the tropical Atlantic (PIRATA). *Bull. Am. Meteorol. Soc.* **1998**, *79*, 2019–2032. [CrossRef]
62. Mcphaden, M.J.; Meyers, G.; Ando, K.; Masumoto, Y.; Murty, V.; Ravichandran, M.; Syamsudin, F.; Vialard, J.; Yu, L.; Yu, W. RAMA: The research moored array for African–Asian–Australian monsoon analysis and prediction. *Bull. Am. Meteorol. Soc.* **2009**, *90*, 459–480. [CrossRef]
63. Väli, G.; Meier, H.E.M.; Elken, J. Simulated halocline variability in the Baltic Sea and its impact on hypoxia during 1961–2007. *J. Geophys. Res. Ocean.* **2013**, *118*, 6982–7000. [CrossRef]
64. D'Ortenzio, F.; Iudicone, D.; de Boyer Montegut, C.; Testor, P.; Antoine, D.; Marullo, S.; Santoleri, R.; Madec, G. Seasonal variability of the mixed layer depth in the Mediterranean Sea as derived from in situ profiles. *Geophys. Res. Lett.* **2005**, *32*. [CrossRef]
65. Tang, W.; Fore, A.; Yueh, S.; Lee, T.; Hayashi, A.; Sanchez-Franks, A.; Martinez, J.; King, B.; Baranowski, D. Validating SMAP SSS with in situ measurements. *Remote Sens. Environ.* **2017**, *200*, 326–340. [CrossRef]
66. Lehmann, A.; Myrberg, K.; Post, P.; Chubarenko, I.; Dailidiene, I.; Hinrichsen, H.H.; Hüssy, K.; Liblik, T.; Meier, H.E.M.; Lips, U.; et al. Salinity dynamics of the Baltic Sea. *Earth Syst. Dyn.* **2022**, *13*, 373–392. [CrossRef]
67. Yueh, S.H.; West, R.; Wilson, W.J.; Li, F.K.; Njoku, E.G.; Rahmat-Samii, Y. Error sources and feasibility for microwave remote sensing of ocean surface salinity. *IEEE Trans. Geosci. Remote Sens.* **2001**, *39*, 1049–1060. [CrossRef]